Learning Friction Model for Magnet-actuated Tethered Capsule Robot

Yi Wang[1,a], Yuyang Tu[2,a], Yuchen He[3], Xutian Deng[1], Ziwei Lei[1], Jianwei Zhang[2] and Miao Li[†1]

***Abstract*— The potential diagnostic applications of magnet-actuated capsules have been greatly increased in recent years. For most of these potential applications, accurate position control of the capsule have been highly demanding. However, the friction between the robot and the environment as well as the drag force from the tether play a significant role during the motion control of the capsule. Moreover, these forces especially the friction force are typically hard to model beforehand. In this paper, we first designed a magnet-actuated tethered capsule robot, where the driving magnet is mounted on the end of a robotic arm. Then, we proposed a learning-based approach to model the friction force between the capsule and the environment, with the goal of increasing the control accuracy of the whole system. Finally, several real robot experiments are demonstrated to showcase the effectiveness of our proposed approach.**

***Keywords*— tethered capsule robot, magnetic actuation, friction model**

I. INTRODUCTION

Capsule endoscopy robots are commonly used for clinical intestinal and stomach inspections. The capsule robot enters the body by being swallowed or being placed into the patient's intestines. Capsule robots are divided into two distinct types: tethered [1] and wireless [2]. The tethered capsule robot has obvious advantages of scalability and repeatability compared with wireless. The tethered can provide a stable video transmission channel and enough light, which can efficiently support the inspection and treatment of the digestive tract, stomach and other parts [3]. To achieve various functions based on the premise that the robot is to be pulled to target-point. The most effective control scheme is the external magnetic field driver [4]. The external magnetic field can be provided in three methods: the permanent magnet-combined current coil [5], the permanent magnet [6] and a three-axis Helmholtz magnetic coil [7].

The external magnetic field driver can effectively overcome the problem that the tethered capsule move passively through peristalsis of the digestive tract. A driving method of hand-held permanent magnet device is proposed in [8], the motor is mounted on the permanent magnet to solve the problem of multi-degree-of-freedom operation. To further explore this problem, new control algorithms based on the manipulator and three translation axis table are proposed in [1] and [5] respectively. However, the key problem of driving control is modeling the tethered. There are some unknown factors in the model of the tethered capsule robot, which generally come from the friction between the tethered and the environment.

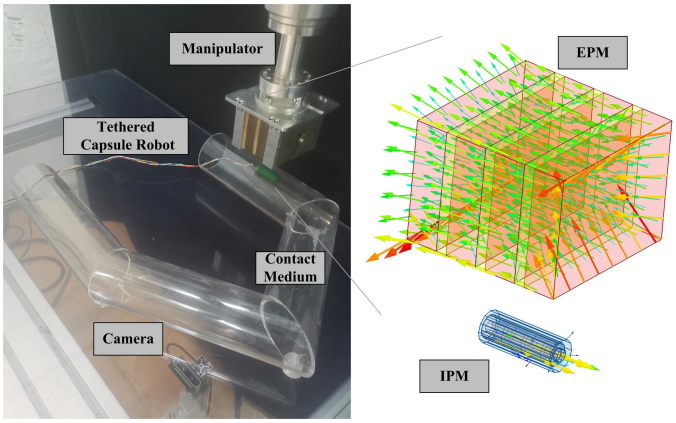

Fig. 1. The picture shows the overall scene and magnetic field of the magnet: At the end of the manipulator is an external permanent magnet (EPM), and an inner permanent magnet (IPM) is inside the terthered capsule robot. Contact medium is an obstacle between IPM and EPM.

In order to analyze the friction factor between the capsule and the environment, the speed of the capsule robot and the resistance model of the intestine was established [9], and the design parameters of the robot capsule endoscope were used in the resistance model [4]. But, these methods cannot obtained the accurate friction force, so Kim *et al.* made a specially designed tribological tester to study the influence of capsule shape on frictional resistance characteristics [10]. A constant velocity friction model was established to study the influence of contact deformation on friction [11]. Despite these model-methods works well in their assumption, these methods had no quantitatively analyzed the friction and drag caused by the tethered. We proposed a learning friction model of the tethered capsule robot in [12], and proved the relationship between friction and the speed of the manipulator in plane motion. However, previous work lacked comparative experiments on the effectiveness of the learning friction model and demand to prove the universality of the method of obtaining the friction model. This article further optimizes the above work.

This paper proposes a dynamic model with friction to

[1] School of Power and Mechanical Engineering, Wuhan University, Hubei, China (e-mail: miao.li@whu.edu.cn)

[2] Department of Informatics, University of Hamburg, Germany (e-mail: yuyang.tu@studium.uni-hamburg.de)

[3] School of Mechanical Engineering and Automation, Wuhan Textile University, Hubei (e-mail: heyuchen2021@outlook.com)

[a] These authors have contributed equally to this work.

† Corresponding author.

This work was supported by the Natural Science Foundation of Jiangsu Province (Grant No. BK20180235) and the German Research Foundation (DFG) and the National Science Foundation of China in project Crossmodal Learning, TRR-169.

compensate for the movement of the tethered capsule robot. First, we analyzed all forces of the tethered capsule robot, including gravity, contact force with mediums, and the tractive-force and friction caused by the tethered. Second, movement data of friction model can be collected from the plane motion between the tethered capsule robot and contact mediums. Furthermore, we obtained the specific friction model of the tethered capsule robot by fitting a scatter plot of sports data. Finally, model-constraints were added between the preset trajectory point speeds of the control algorithm, which limited the speed of the external magnetic drive devise within the effective speed range of the friction model. The trajectory tracking error of the capsule robot and the fluctuation of the contact force can be significantly reduced under the application of the friction model.

The main contribution of our research is to propose a friction model learning method, which has the potential to apply motion control to the tethered capsule robot in mediums with any friction coefficient. In addition, the article provides a plane experiment method to obtain friction model of the tethered capsule robot, and further guides the capsule movement control. The organizational structure of this paper is as follows: In Section II, the theory of capsule friction model is proposed. In Section III, the entire experimental system, magnetic field simulation method and the process of obtaining the friction model are introduced. In Section IV, the validity of the friction theory in the current experimental environment is verified through experiments. In Section V, the whole research work and results of this article are summarized.

II. Problem Statement

The key to control the tethered capsule is the modeling of the tethered capsule system. Fig. 2 shows the force diagram of the tethered capsule during the capsule motion. A friction dynamic model between the capsule robot and the contact interface is proposed to optimize the motion control of the capsule robot attached to different mediums [11], [13], [14]. We expect to obtain a more specific friction relationship between the capsule robot and the environment to improve the control accuracy.

A. Dynamic Model of Magnetron Capsule

According to the application of the point dipole model in [7], [11], the theoretical dynamic model of magnetron capsule is defined as:

$$B(x)\ddot{x} + C(x,\dot{x})\dot{x} + G(x) = \tau_m(x,q) \tag{1}$$

where $x \in \mathbb{R}^3$ is the capsule pose (position and orientation) and $q \in \mathbb{R}^6$ represents the robot joint variables; matrices $B(x)$, $C(x,\dot{x})$, $G(x)$ are the inertia, Coriolis matrix and gravity of the capsule respectively. The vector $\tau_m(x,q) \in \mathbb{R}^6$ represents the magnetic force and torque exerted by the EPM on the IPM, which is highly non-linear. Our aim is to find q such that x approaches a desired value x_d.

In order to get a controllable position control scheme, the differential of (1) can be deduced as the following

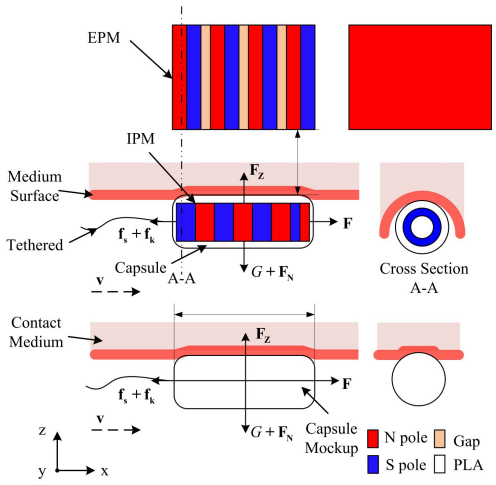

Fig. 2. The force diagram of the magnetron capsule.

expression:

$$\dot{\tau}_m = \frac{\partial \tau(x,q)}{\partial x}\dot{x} + \frac{\partial \tau(x,q)}{\partial q}\dot{q} = J_x\dot{x} + J_q\dot{q} \tag{2}$$

J_x and J_q are derived in the [11], τ_m is the state variable of the control system [11]. Other parameters are shown in Table I. The dynamic model with friction compensation of the magnetron capsule can be expanded to (3) by combining (1) and (2):

$$\begin{cases} B(x)\ddot{x} + C(x,\dot{x})\dot{x} + G(x) = \tau_m(x,q) \\ \dot{\tau_m}(x,q) = J_x\dot{x} + J_q\dot{q} + \dot{\kappa} \end{cases} \tag{3}$$

B. Friction Model Establishment

The $\dot{\kappa}$ mentioned in (3) is put as equivalent to a straight connecting rod in the simulation environment [11], which is not verified in the current research. In the real environment, $\dot{\kappa}$ is judged to represent the friction between the capsule and the environment, including kinetic friction force $\mathbf{f_k}$ and static friction force $\mathbf{f_s}$. The theoretical kinetic model of magnetron capsules can be expressed as (Other parameters are shown in Table I):

$$\begin{gathered} \mathbf{F}+\mathbf{f_s}+\mathbf{f_k}=m\mathbf{a},\ \mathbf{f_k}=\mathbf{F_N}\cdot\mu \\ \mathbf{F}+\mathbf{f_s}+\mathbf{F_N}\cdot\mu=m\mathbf{a} \end{gathered} \tag{4}$$

In particular, kinetic friction and static friction have been proved to be relative. These two concepts can be replaced by a view of rate-dependent friction, the law of friction of rocks [14], which is generally applicable to materials including polymers, glasses, etc. In [14], the coefficient of friction is related to instantaneous velocity $\mathbf{v}$ and state variable θ.

$$\mu = \mu_0 - a\ln\left(\frac{\mathbf{v}^*}{|\mathbf{v}|}+1\right) + b\ln\left(\frac{\mathbf{v}^*\theta}{\mathbf{D_c}}+1\right) \tag{5}$$

$|\mathbf{v}| << \mathbf{v}^*$, the expression of friction law (5) can be rewritten as:

$$\mu = \mu_0 - (a-b)\ln\left(\frac{\mathbf{v}^*}{|\mathbf{v}|}+1\right) \tag{6}$$

We assume c is the relationship $(a-b)$ that is a friction factor of the friction model, so the friction model can be predicted by substituting (6) into (4):

$$\mathbf{F}+\mathbf{f_s}+\mathbf{F_N}\cdot\left[\mu_0 - c\cdot\ln\left(\frac{\mathbf{v}^*}{|\mathbf{v}|}+1\right)\right] = m\mathbf{a} \tag{7}$$

TABLE I
NOMENCLATURE USED

Symbol	Description
κ	All friction between capsule and Environment
$\mathbf{F}$	Traction Force of capsule in Movement Direction
$\mathbf{F_z}$	Magnetic Force of capsule in Vertical Direction
$\mathbf{F_N}$	Supporting Force of capsule in Vertical Direction
$\mathbf{f_s}$	Static Friction Force
$\mathbf{f_k}$	Kinetic Friction Force
m	Capsule Mass (20.9g)
$\mathbf{a}$	Capsule Acceleration
$\mathbf{v}$	Manipulator Speed (Preset Experimental Speed)
$\mathbf{v}^*$	The Typical Speed, about 0.2m/s [13]
$\mathbf{D_c}$	Critical Slip Length [13]
a	System Constant [13], [14]
b	System Constant [13], [14]
μ_0	Sliding Friction Coefficient
c	Equation of Friction System to be Solved.

III. EXPERIMENT

A. Experimental System Setup

As shown in Fig. (3), the overall hardware system mainly consists of EPM, IPM and manipulator. At present, permanent magnet is one of the most commonly used approach to provide stable and strong magnetic field, whose shapes mainly include cylinder [5], ring [6] and cube [15]. The EPM terminal designed in this paper is composed of four strong cubic magnets in a Halbach Array [12] which can be applied to increase magnetic field range and strength shown in Fig. (3)(b). EPM is connected to the manipulator through 6061 aluminum alloy to avoid the influence of strong magnetism. As shown in Fig. 3(c), the IPM design is largely inspired by the work in [16], and in our case a tethered robot is used. The weight, length, and diameter of the capsule robot are 20.9g, 36mm, and 14mm respectively. The detailed structure of the tethered capsule robot is shown in Fig. 3(c). During the movement, the capsule robot is attached to the PVC plate by the external magnetic force. A transparent PVC plate is supposed to facilitate camera calibration and collect the motion information of the capsule robot.

As shown in (7), the friction model established in this paper can be applied to mediums with different sliding friction coefficients. According to the friction coefficient between PVC [17] and PLA [18] and the test tension range of the relative movement of PLA and PVC is 0.042∼0.048N, we set the sliding friction coefficient of PVC transparent plate and capsule robot as 0.22. After the same processes are repeated on paper and polyester-cloth, we get that the friction coefficient of the robot on paper is 0.26 [19], and the friction coefficient on polyester-cloth is 0.19 [20].

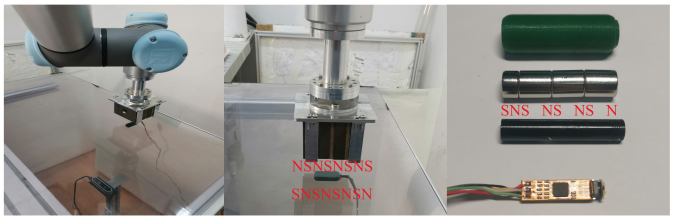

Fig. 3. Structure of system: (a) Schematic diagram of the overall scene. (b) Working diagram of EPM and IPM. (c) A detail drawing of the capsule robot.

B. Acquire $\mathbf{F}$ and $\mathbf{F_z}$ in Friction Model

The drag force $\mathbf{f_s}$ of the system is measured using the tension dynamometer, which is 0.03N. $\mathbf{F}$ and $\mathbf{F_z}$ are obtained by theoretical simulation (Fig. (4)). From (7), the ambient friction force of the capsule robot can be compensated by adjusting $\mathbf{v}$ the velocity of the manipulator, to determine the force of the capsule robot. In this way, the instantaneous acceleration of the capsule robot can be controlled, but this friction relation c must be determined in advance, the detailed acquisition steps are as follows.

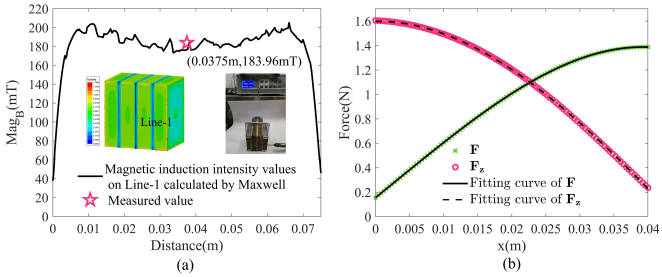

Fig. 4. Results of finite element analysis: (a) Comparison of simulated and measured values. (b) Simulation value and fitting curve of $\mathbf{F}$ and $\mathbf{F_z}$.

The steps for Maxwell to acquire $\mathbf{F}$ and $\mathbf{F_z}$ are as follows: First, the field source IPM and EPM are processed by the equivalent volume current method. Then the magnetic field distribution is obtained according to the homogeneous wave equations. Finally, the electromagnetic force [21] on the IPM is calculated based on the principle of virtual work, which can be given by:

$$\mathbf{F} = \frac{dW}{d\mathbf{s}} = \frac{\partial}{\partial \mathbf{s}}\left[\int_V\left(\int_0^H \mathbf{B}\cdot d\mathbf{H}\right)dV\right] \tag{8}$$

where $d\mathbf{s}$ is virtual displacement, W is the total magnetic field energy of the system, V is the volume of the IPM, $\mathbf{B}$

is the magnetic flux density, and $\mathbf{H}$ is the magnetic field strength.

To verify the validity of the simulation parameters settings (see Table II). We compared the value of magnetic induction measured by maxwell and Gauss meter on Line-1 of the field source EPM (see Fig 4(a)). The relative error between the simulation results and the measured data is 4.11%. The values of $\mathbf{F}$ and $\mathbf{F_z}$ (see Fig 4(b)) on the IPM are calculated by the three-dimensional transient solver when the EPM moves in the x-direction at a constant speed of 0.01m/s. With the force trend of the simulation calculation results, the relationship between the electromagnetic force and the relative distance is obtained by polynomial fitting [22] (see Fig 4(b)). The root mean squared errors (RMSE) fitted by $\mathbf{F}$ and $\mathbf{F_z}$ are 0.068% and 0.294%, respectively.

TABLE II
PARAMETERS OF EPM AND IPM

Parameter	EPM	IPM
Effective Length (mm)	60	35
Effective Width / Outer Diameter (mm)	75	$D10$
Effective Height / Internal Diameter (mm)	55	$D6$
Material	NdFe30	NdFe30

C. Acquire $\mathbf{v}$ and $\mathbf{a}$ in Friction Model

The coordinates of the end of the manipulator and the capsule robot are recorded at the same frequency (20Hz). Fig. 5(a)-(d) shows the capsule trajectory tracking process. The velocities $\mathbf{v}$ of EPM and IPM can be calculated by $\frac{\Delta(\mathbf{P}_\chi - \mathbf{P}_{\chi-1})}{\Delta t}$ after each point in the trajectory is recorded. χ indicates the time step. The coordinate data of the EPM ($\mathbf{P_E} \in \mathbb{R}^3$) at the end of the robotic arm are directly read from the ROS node. The tethered capsule robot acceleration $\mathbf{a}$ can be obtained by calculating $\frac{\Delta(\mathbf{V}_\chi - \mathbf{V}_{\chi-1})}{\Delta t}$, where ($\mathbf{P_I} \in \mathbb{R}^3$) is the coordinate information of the capsule robot collected by the camera. The friction model of the tethered capsule can be analyzed more scientifically by collecting movement data in four directions: up, down, left, and right. The data points above in each movement are collected with at 10s intervals to reduce random errors. Detail is shown in Fig. 6.

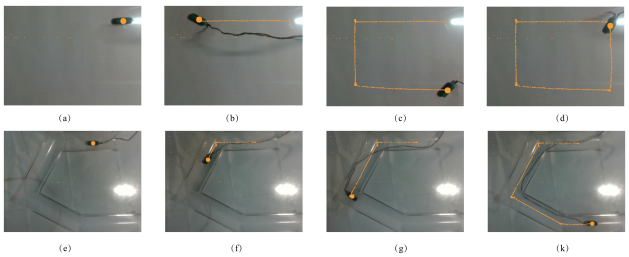

Fig. 5. The trajectory tracking process of the capsule robot: (a)-(d) The rectangular trajectory of the capsule robot. (e)-(k) Bend pipe trajectory of the capsule robot.

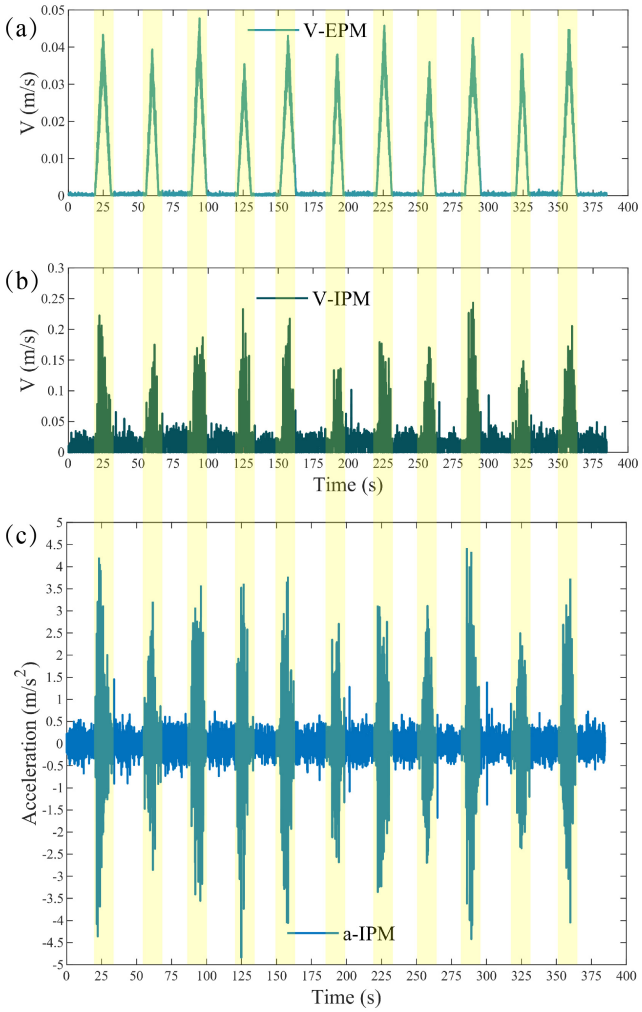

Fig. 6. (a) shows the $\mathbf{v}$ of EPM. (d) shows the $\mathbf{v}$ of IPM. (c) shows the $\mathbf{a}$ of the IPM. Yellow shaded areas represent 10s line-move on the surface of PVC.

D. Obtaining c in Friction Model.

To ensure the rationality of the parameters in the given friction model, the coordinates of the end of the manipulator and the capsule robot are delivered and saved at the same frequency. The red line in Fig.7 indicates the target trajectory of the manipulator. The IPM follows the EPM movement, which tracks point information is collected by the camera. At the same time, the coordinate information of IPM and EPM is saved in the same program based on time series. By substituting the distance of each ($\mathbf{P_E}$-$\mathbf{P_I}$) into the Maxwell simulation [21], $\mathbf{F}$ and $\mathbf{F_z}$ at the corresponding time can be obtained.

In order to learn the friction model in (7), we repeat the above process to obtain more than 20000 track point ($\mathbf{P_E}$ and $\mathbf{P_I}$) data (including $\mathbf{F}$, $\mathbf{F_z}$ and $\mathbf{a}$). The plane test trajectory diagrams of the three mediums are as follows. All $\mathbf{v}$-c points obtained above are plotted in the rectangular coordinate-system. We found that these scatter-charts were in line with the rule of multi-term function distribution, so polynomial curve fitting [22] is used to fit and set multi-

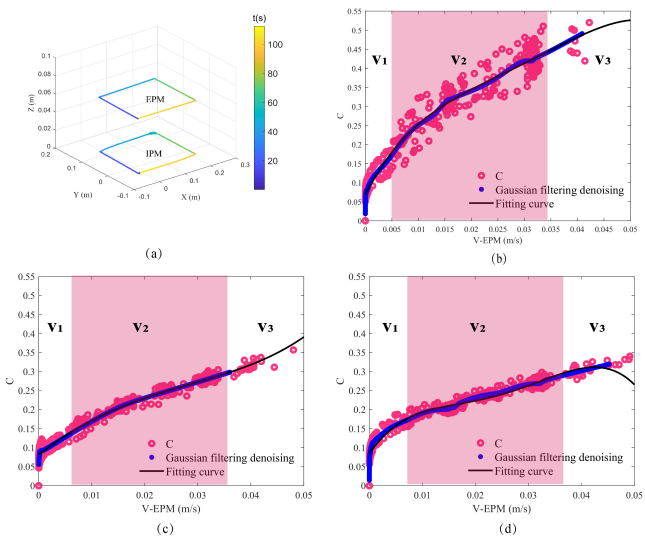

Fig. 7. (a) shows the trajectory of capsule robot and manipulator based on time series. (b), (c), (d) represents the three media movement trajectory collection points respectively, and the factor expression fitting function of the friction model obtained. The red shaded area indicates the effective speed range guided by the friction model.

order derivatives for the scatter-charts (as shown in Fig. 7(b)-(d)). As a result, the fifth-degree polynomial of $\mathbf{v}$ could fit c with small error (The sum variance between $\mathbf{v}$-c and the fifth-degree polynomial is 0.053 when the control speed of the manipulator is between 0.005m/s and 0.04m/s on the PVC). Similarly, the three friction model formulas in different materials are obtained by matlab simulation set. The specific fitting relationship is represented by:

$$c = p_1 * \mathbf{v}^4 + p_2 * \mathbf{v}^3 + p_3 * \mathbf{v}^2 + p_4 * \mathbf{v} + p_5 \qquad (9)$$

The values of p_1, p_2, p_3, p_4 and p_5 are listed in Table III.

TABLE III

VALUES OF p_1, p_2, p_3, p_4, p_5

Type	p_1	p_2	p_3	p_4	p_5
PVC	-1.943×10^5	2.318×10^4	-1018	26.36	0.0699
paper	2.386×10^4	8.069×10^2	-190.6	10.72	0.08173
polyester-cloth	-3.75×10^5	3.692×10^4	-1232	19.79	0.08508

IV. Experimental Results and Discussion

A. Test Results of Friction model

The control experiment group is designed to test the friction model obtained in (7). The evaluation indicators of the control experimental group are trajectory tracking error and pressure change. Effective speed and friction factors are given in (9). Specific implementation scheme is organized as follows: the capsule robot repeats same motions in the same pipeline at three different speeds. Contrast tests have been carried out on smooth pipes, paper surfaces, and polyester-cloth surfaces, as shown in the actual movement scene in Fig. 8(a)-(c).

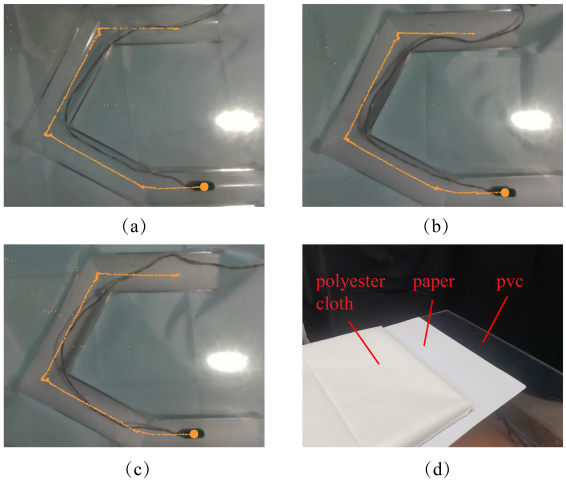

Fig. 8. The contact medium of (a) is PVC, the contact medium of (b) is paper, and the contact medium of (c) is polyester-cloth. (d) is a schematic diagram of the three materials.

TABLE IV

AVERAGE ACCURACY (TRAJECTORY TRACKING ERROR) OF $\mathbf{v_1}$, $\mathbf{v_2}$, $\mathbf{v_3}$ UNDER THREE MEDIUMS

Error (mm)	$\mathbf{v_1}$	$\mathbf{v_2}$	$\mathbf{v_3}$	**Improvement**
PVC	7.21	6.91	7.41	4.16% / 6.75%
paper	7.15	6.72	7.33	6.01% / 8.32%
polyester-cloth	7.05	6.63	7.17	5.95% / 7.43%

$\mathbf{v_1}$, $\mathbf{v_2}$ and $\mathbf{v_3}$ represent three different velocity values on the left, middle and right of the velocity range of the friction model (as shown in Fig. 7). The values of the test speed of each medium ($\mathbf{v_1}$, $\mathbf{v_2}$ and $\mathbf{v_3}$), see Supplementary Video for details. As is shown in Fig. 8, we attach paper and cloth to the inside of the pipe to change the coefficient of friction. Table IV shows the improvement of average accuracy of $\mathbf{v_2}$ relative to $\mathbf{v_1}$ and $\mathbf{v_3}$ in three mediums respectively, and the values of trajectory tracking error on PVC are shown in Fig. 9 (b). To calculate the stability of contact force, the 1N scale-line is regarded as the standard line for the fluctuation of the contact force at the collection points in the whole trajectory. The contact force improvement of $\mathbf{v_2}$ on PVC is 6.12% and 6.47% compared with $\mathbf{v_1}$ and $\mathbf{v_3}$ respectively. The fluctuation of contact force on PVC is shown in Fig. 9(c). The contract force data between paper (and polyester-cloth) and the tethered capsule robot see Supplementary Video.

B. Discussion

The friction model in this paper can be applied to improve the accuracy obviously compared the trajectory tracking error (7.04mm) of Zhang, P *et al.* [23]. The validity of the friction model is verified with different contact mediums shown in Fig. 8. In the future, the contact force in current experimental scene is nearly a simulation to the actual working process of the capsule. Future work is planned as follows: First, force estimation will be added into the system to facilitate force control [24]. Second, the system will be further verified

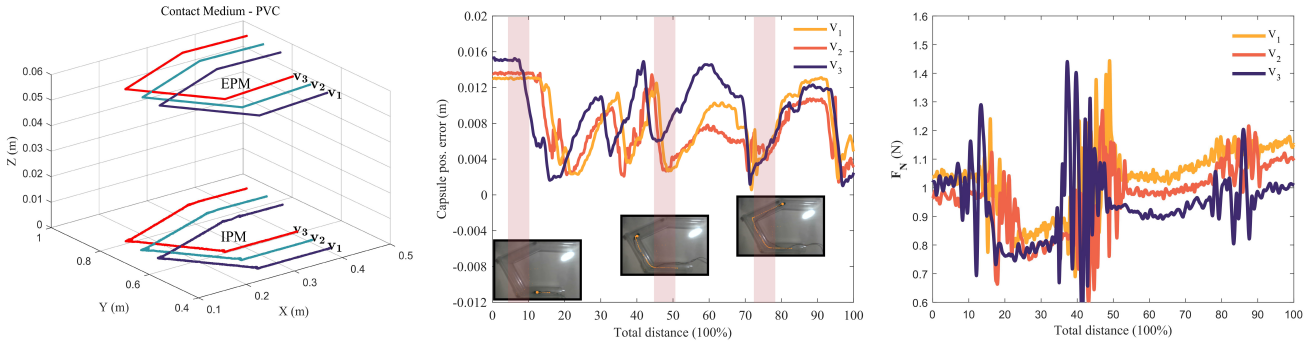

(a) (b) (c)

Fig. 9. The picture shows the tethered capsule robot motion on the PVC with $\mathbf{v_1}$,$\mathbf{v_2}$,and $\mathbf{v_3}$, which are 0.005m/s, 0.012m/s, 0.035m/s respectively. (a) The trajectory graph of 10 average values of 3 sets of speed. The same color is a set of EPM and IPM trajectory control groups. (b) shows the trajectory tracking error at the three speeds of PVC. The three shaded areas from left to right correspond to the starting segment, the second corner, and the third corner, respectively. (c) Contact force fluctuations at three speeds.

in animal tissues. Third, a more compact structure will be designed for the system.

V. CONCLUSION

This research proposes a learning friction model for the magnet-actuated tethered capsule robot that is suitable for plane and space, and provides a method to obtain the model. The friction models of three mediums provide effective speed ranges respectively. The tethered capsule robot can improve the trajectory tracking error and contact force stability within the effective speed range. In addition, three contact motions with different friction coefficients show the universal applicability of this learning friction model method. We can get the specific relationship of the tethered capsule between the control speed $\mathbf{v}$ and the friction factor c during the plane movement in advance.

REFERENCES

[1] P. R. Slawinski, A. Z. Taddese, K. B. Musto, S. Sarker, P. Valdastri, and K. L. Obstein, "Autonomously controlled magnetic flexible endoscope for colon exploration," *Gastroenterology*, vol. 154, no. 6, pp. 1577–1579, 2018.

[2] P. Valdastri, M. Simi, and R. J. Webster III, "Advanced technologies for gastrointestinal endoscopy," *Annual review of biomedical engineering*, vol. 14, pp. 397–429, 2012.

[3] S. S. Mapara and V. B. Patravale, "Medical capsule robots: A renaissance for diagnostics, drug delivery and surgical treatment," *Journal of Controlled Release*, vol. 261, pp. 337–351, 2017.

[4] L. J. Sliker, G. Ciuti, M. E. Rentschler, and A. Menciassi, "Frictional resistance model for tissue-capsule endoscope sliding contact in the gastrointestinal tract," *Tribology International*, vol. 102, pp. 472–484, 2016.

[5] G. Pittiglio, L. Barducci, J. W. Martin, J. C. Norton, C. A. Avizzano, K. L. Obstein, and P. Valdastri, "Magnetic levitation for soft-tethered capsule colonoscopy actuated with a single permanent magnet: A dynamic control approach," *IEEE robotics and automation letters*, vol. 4, no. 2, pp. 1224–1231, 2019.

[6] A. W. Mahoney and J. J. Abbott, "Five-degree-of-freedom manipulation of an untethered magnetic device in fluid using a single permanent magnet with application in stomach capsule endoscopy," *The International Journal of Robotics Research*, vol. 35, no. 1-3, pp. 129–147, 2016.

[7] M. Salehizadeh and E. Diller, "Three-dimensional independent control of multiple magnetic microrobots via inter-agent forces," *The International Journal of Robotics Research*, vol. 39, no. 12, pp. 1377–1396, 2020.

[8] G.-S. Lien, C.-W. Liu, J.-A. Jiang, C.-L. Chuang, and M.-T. Teng, "Magnetic control system targeted for capsule endoscopic operations in the stomach—design, fabrication, and in vitro and ex vivo evaluations," *IEEE Transactions on Biomedical Engineering*, vol. 59, no. 7, pp. 2068–2079, 2012.

[9] C. Zhang, H. Liu, R. Tan, and H. Li, "Modeling of velocity-dependent frictional resistance of a capsule robot inside an intestine," *Tribology Letters*, vol. 47, no. 2, pp. 295–301, 2012.

[10] N. Baek, I. Sung, and D. Kim, "Frictional resistance characteristics of a capsule inside the intestine for microendoscope design," *Proceedings of the Institution of Mechanical Engineers, Part H: Journal of Engineering in Medicine*, vol. 218, no. 3, pp. 193–201, 2004.

[11] B. Guo, Y. Liu, and S. Prasad, "Modelling of capsule–intestine contact for a self-propelled capsule robot via experimental and numerical investigation," *Nonlinear Dynamics*, vol. 98, no. 4, pp. 3155–3167, 2019.

[12] Y. Wang, Y. He, X. Deng, Z. Lei, Y. Chen, and M. Li, "Learning friction model for tethered capsule robot," *arXiv preprint arXiv:2108.07151*, 2021.

[13] K. Knothe, "Contact mechanics and friction: physical principles and applications," 2011.

[14] C. Marone, "Laboratory-derived friction laws and their application to seismic faulting," *Annual Review of Earth and Planetary Sciences*, vol. 26, no. 1, pp. 643–696, 1998.

[15] H. Allag, J.-P. Yonnet, and M. E. Latreche, "3d analytical calculation of forces between linear halbach-type permanent-magnet arrays," in *2009 8th International Symposium on Advanced Electromechanical Motion Systems & Electric Drives Joint Symposium*. IEEE, 2009, pp. 1–6.

[16] M. Gao, C. Hu, Z. Chen, H. Zhang, and S. Liu, "Design and fabrication of a magnetic propulsion system for self-propelled capsule endoscope," *IEEE Transactions on Biomedical Engineering*, vol. 57, no. 12, pp. 2891–2902, 2010.

[17] K. Giannoukos and K. Salonitis, "Study of the mechanism of friction on functionally active tribological polyvinyl chloride (pvc)–aggregate composite surfaces," *Tribology International*, vol. 141, p. 105906, 2020.

[18] S. Zhiani Hervan, A. Altınkaynak, and Z. Parlar, "Hardness, friction and wear characteristics of 3d-printed pla polymer," *Proceedings of the Institution of Mechanical Engineers, Part J: Journal of Engineering Tribology*, vol. 235, no. 8, pp. 1590–1598, 2021.

[19] A. Johansson, C. Fellers, D. Gunderson, and U. Haugen, "Paper friction–influence of measurement conditions," *Tappi journal*, vol. 81, no. 5, pp. 175–184, 1998.

[20] M. Robins, R. Rennell, and R. Arnell, "The friction of polyester textile fibres," *Journal of Physics D: Applied Physics*, vol. 17, no. 7, p. 1349, 1984.

[21] J. Ku, J. Xia, J. Li, X. Peng, B. Guo, and H. Ran, "Accurate calculation of major forces acting on magnetic particles in a high-gradient magnetic field: A 3d finite element analysis," *Powder Technology*, 2021.

[22] V. MATLAB, "9.3. 0.713579 (r2017b)," *The Math-Works Inc., Natick, MA*, 2017.

[23] P. Zhang, J. Li, W. Zhang, Y. Hao, G. Ciuti, T. Arai, P. Dario, and Q. Huang, "Endoluminal motion recognition of a magnetically-guided capsule endoscope based on capsule-tissue interaction force," *Sensors*, vol. 21, no. 7, p. 2395, 2021.
[24] X. Gao, J. Ling, X. Xiao, and M. Li, "Learning force-relevant skills from human demonstration," *Complexity*, vol. 2019, 2019.